ACS APPLIED POLYMER MATERIALS

pubs.acs.org/acsapm Article

Highly Porous Curcumin-Loaded Polymer Mats for Rapid Detection of Volatile Amines

Despoina Kossyvaki, Aurelio Barbetta, Marco Contardi, Matteo Bustreo, Katarzyna Dziza, Simone Lauciello, Athanassia Athanassiou, and Despina Fragouli*

Cite This: https://doi.org/10.1021/acsapm.2c00418 Read Online

ACCESS | Metrics & More | Article Recommendations | Supporting Information

ABSTRACT: Here, the development of highly porous colorimetric indicators that are able to rapidly sense the presence of amine vapors is presented. Specifically, porous, curcumin-loaded polycaprolactone fibers are formed by electrospinning through non-solvent-induced phase separation. In comparison to the non-porous fibers, the developed system shows significantly higher sensitivity and responsivity to the presence of dimethylamine vapors, with a distinct color change at very low vapor concentrations (2.33 ppm compared to 9.26 ppm) within the first 5 s of exposure. Indeed, CIELAB analysis proves that the induced color changes can be easily perceived visually, as the differences between the initial and the final color of the indicator after its interaction with the modified environment are well above the limit for visual perception, even by inexperienced users. Furthermore, the color changes are reversible, enabling the use of the same indicator several times, making it, thus, a sustainable colorimetric indicator system that can be used in applications where the rapid detection of low concentration of alkaline vapors is necessary.

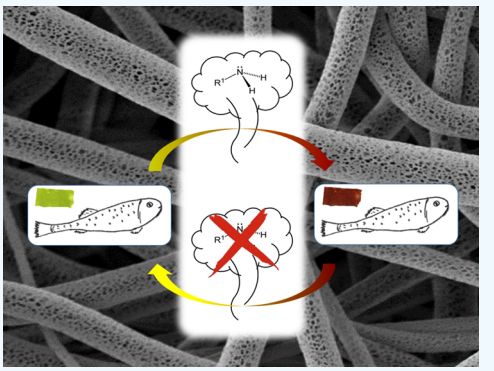

KEYWORDS: *porous electrospun fibers, gas sensing, intelligent packaging, pH indicators, dimethylamine*

1. INTRODUCTION

Microorganisms that are limited in small populations naturally live, multiply, and metabolize various substances in food. Among the by-products of microbial metabolism, amines are nitrogenous, organic compounds that are created by the decarboxylation of amino acids or amination and transamination of aldehydes or ketones.[1] These low molecular weight metabolic products are normally present in very low concentrations in the tissues of bodies with biological activity, such as food products derived from animals (fish, meat, etc.).[2] However, bad processing and inadequate storage conditions may result in premature food spoilage, as specific types of microorganisms colonize and grow in an uncontrolled way due to the favorable ambient conditions. These microorganisms produce high amounts of off-flavor compounds[3] such as trimethylamine (TMA), dimethylamine (DMA), and biogenic amines (BAs), through their metabolic activity. Compounds such as TMA and DMA, along with other primary, secondary, tertiary amines and ammonia, constitute the total volatile basic nitrogen (TVB-N), which increases with the putrefaction progress during the deamination of amino acids of protein-based food. The existence of TVB-N in high concentrations has been also correlated with high quantities of BAs.[4] In such high quantities, these substances have been implicated as a major causative agent of foodborne diseases such as intoxication.[5] Hence, it is important to monitor these toxins in order to evaluate the freshness of protein-based food products[6] and to determine whether the food is spoiled.

Amines and such off-flavor compounds can alter the pH of the environment in which they are found due to their alkaline nature; therefore, a way to trace them is through pH monitoring.[7] For this reason, the recently developed pH indicators can be introduced directly in the headspace of the food package in order to provide qualitative or semi-quantitative information of the presence of the microorganisms in the food, indicating its quality through visual colorimetric changes.[8] To do so, molecules able to present a different hue, depending on the pH of the environment, have been investigated and used as principal components of these indicators, with natural molecules being the most recent and prevalent preference, mainly due to their biocompatible and sustainable essence.[9−13]

A popular natural pH-sensitive molecule is curcumin, a linear polyphenolic compound and natural food pigment that can be extracted from the rhizome of turmeric (*Curcuma longa* and *Curcuma domestica*). As presented in Figure S1 of the

Received: March 11, 2022
Accepted: May 5, 2022

Supporting Information, it consists of two *o*-methoxy phenolic groups connected by a seven-carbon linker, an α,β-unsaturated β-diketo moiety. The diketo group exhibits keto−enol tautomerism and can exist in different types of conformers depending on the nature of the environment with which it interacts. Curcumin has a yellow color in acidic and neutral environments (pH = 3−7), with the keto form predominating and acting as an extraordinarily potent H-atom donor. In alkaline environments (pH ≥ 8) the enol form, which acts as an electron donor, predominates and curcumin appears red-orange.[14]

Thanks to this behavior, curcumin has been used to fabricate colorimetric pH indicators for food packaging applications, alone[9] or combined with other pH-sensitive dyes,[15] in order to indicate the presence of amines[16] and therefore the food condition. To do so, polymer-based solid-composite structures in the form of films,[15,17−25] hydrogels,[26] fibers,[9,25,27−29] and other structures[30] that can be applied in the headspace of the package have been developed. However, as in the case of other types of colorimetric indicators developed for food packaging, there are several challenges that still need to be tackled to reach a feasible, well-performing system.[31] For example, some of the developed indicators are not able to present color changes that can be easily detected.[17,21] Others, even if they are clearly changing color over time in the presence of spoiled food,[27] they do not directly correlate the visual perceivable color change with the real condition of the food and with the concentration of amines above which this change occurs, apart from very few cases.[9,28,32] In other cases, the color change due to the interaction with a defined concentration of amines is not visible enough.[12] Moreover, the evaluation of pH-induced color changes of the indicators upon their immersion into buffer solutions,[20,30,33] the generic tests with vapors of fixed concentrations without further investigation (i.e., limit of detection, realistic spoilage vapor concentrations, time of response, etc.),[19,23,26,29,34] the lack of testing with specific off-flavor compounds responsible for microbial food spoilage,[35] the demo tests with food without verification of its spoilage,[27] and the missing color reversibility studies[15,19,27] are some of the limitations of the previous studies. These inadequacies may guide to misleading information, as the food may be spoiled way before the color change of the indicator, either because this occurs at amine concentrations higher than the ones of the spoilage limit or due to the indicator's mismatching response time. Therefore, colorimetric indicators with improved sensitivity and with real-time monitoring capability able to precisely indicate the limit above which the food is unsuitable for consumption should be performed.

To address these challenges, materials with high available active surface areas should be explored that are able to efficiently interact and, subsequently, change color distinctly in the presence of amine compounds of defined concentration. To this aim, porous materials with high active surface area[34] may guarantee this efficient interaction, which prompts faster responses and higher sensitivity with respect to films fabricated by the same starting materials.[36] Although some steps are performed toward this direction with the fabrication of pH-sensing foams or fibrous mats,[9,33,34,37−41] the responsive capability of the porous systems could be further improved by inducing the formation of additional porosity on the surface of the pore walls[42] or of each fiber,[43] enhancing their active surface area.[44] Nonetheless, to the authors' knowledge, although the porous fibers are used in various fields such as filtration[45] and biomedicine,[46] their utilization as colorimetric food spoilage indicators has not been reported yet. Along with that, the reusability of the indicators, a so-far non-sufficiently studied aspect, could pave the way for an alternative type of colorimetric indicators able to rapidly denote the food spoilage and be reutilized various times, even in a domestic environment using a controlled compact kit.

Hence, we present the development of highly porous curcumin−polycaprolactone fibrous mats for the rapid, highly efficient, and repeatable interaction with amine vapors, and we propose this material as a colorimetric indicator for food spoilage. The porous fibers are formed by electrospinning via the non-solvent-induced phase separation process.[43] The stability, porosity, robustness, and wetting properties of the generated mats are explored and compared with the pure polymeric systems, demonstrating that the presence of curcumin does not affect significantly the overall properties of the porous polymeric fibers. To demonstrate the importance of the high porosity on the responsiveness and sensitivity of the curcumin-based colorimetric indicators, comparative studies with non-porous equivalent fiber mats have been performed using basic dimethylamine vapors as a model system. Furthermore, their reversibility and reusability are thoroughly investigated with detailed vapor exposure tests. Through such a detailed study, we prove the efficiency of this material for applications requiring a highly sensitive colorimetric indication approach.

2. MATERIALS AND METHODS

2.1. Materials. Curcumin from *C. longa* (turmeric) powder, polycaprolactone (PCL) (M_n ≈ 80,000 Da), chloroform (≥99.8%), acetone (≥99.5%), ethanol (96%), dimethyl sulfoxide (DMSO) (≥99.5%), cadaverine (CAD), (95%), histamine (HIS) (≥97.0%), DMA (∼40 wt % in H_2O), TMA [∼43-49 wt % in H_2O (T)], ammonium hydroxide solution (30%), and putrescine (PUT), (analytical standard) were purchased by Sigma-Aldrich and used without further purification.

2.2. Fabrication of the Fibers. Electrospinning solutions were prepared by combining PCL with curcumin (0.5 and 1.0 % wt with respect to the polymer). In particular, a mixture of chloroform (boiling point ≈ 61.2 °C) and acetone (boiling point ≈ 56.0 °C) (7:3 chloroform/acetone volume ratio) was prepared which was acting as the PCL solvent. Then, DMSO (boiling point ≈ 189.0 °C) was added to the mixture (9.0% v/v with respect to the final solvent mixture). Subsequently, the PCL was added to the mixture (15.0% w/v) and stirred at room temperature (RT) until its complete dissolution. Such a mixture of solvents with very different boiling points is responsible for the formation of the pores in the electrospun fibers.[47] For the PCL−curcumin solutions, curcumin in the aforementioned concentrations was added to the PCL solutions. Such solutions were electrospun with a vertical electrospinning system using the following optimized parameters: flow rate, 3 mL/h; applied voltage, 17 kV; distance of the aluminum collector from the spinneret tip, 31 cm; temperature, 21−23 °C; and relative humidity, 53−57%. Following this process, mats of PCL and PCL−curcumin 0.5 and 1.0 % wt were formed and named PCL, PCLCU05, and PCLCU1, respectively.

For comparison reasons, samples of non-porous PCL fibers loaded with curcumin 1.0% wt with respect to the polymer, named PCLCU1-NP, were also fabricated starting from a solution of PCL (15.0% w/v), in a mixture of chloroform, acetone (7:3 v/v), and ethanol (9.0% v/v with respect to the final mixture). In this case, the electrospinning parameters were: flow rate, 5 mL/h; applied voltage, 20 kV; distance of the aluminum collector from the spinneret tip, 35 cm; temperature, 21−23 °C; and relative humidity, 26−35%.

2.3. Characterization of the Fibers. *2.3.1. Morphology.* The morphology of the single fibers and of the mats was analyzed using a

https://doi.org/10.1021/acsapm.2c00418
ACS Appl. Polym. Mater. XXXX, XXX, XXX−XXX

JEOL JSM-6490L scanning electron microscope (SEM) and a field emission scanning electron microscope (FE-SEM, JSM 7500 FA). The images were acquired with a secondary electron imaging mode and an acceleration voltage of 10 and 5 kV, respectively, for SEM and FE-SEM analysis. Before imaging, samples were coated with a 10 nm gold layer using a high-resolution sputter coater (Cressington 208 HR).

2.3.2. Pore Structure. The specific surface area (S_{BET}) and the pore size distribution of the samples were evaluated by measurements of nitrogen (N_2) physisorption and mercury intrusion porosimetry (MIP). The complementary information acquired provides a description of the overall porous structure of the electrospun fibrous mats. Prior to the MIP, the skeletal density of the samples was defined with a helium pycnometer (Pycnomatic Evo, Thermo Fisher Scientific), at temperature (T): 20 °C, with a reference volume (i.e., sample compartment) of 4 cm^3, and the assumption that all the open pores were accessible to helium. Ten measurements were performed for each sample with an accuracy of ±0.6%. The skeletal density obtained was then used to calculate the effective porosity and pore size distribution of the mats in the macropore range using a Pascal 140 Evo and a Pascal 240 Evo MIP porosimeters (Thermo Fisher Scientific). The measurements were acquired in two stages: the first was the low-pressure mode (0.001−0.140 MPa) and the second the high-pressure one (0.1−200.0 MPa). Results from both stages were combined to an equivalent pore size range of 0.01−1000.00 μm and analyzed using the SOL.I.D Evo software by the Washburn's equation, assuming a mercury contact angle of 140° and a mercury surface tension of 0.48 N m^{-1}, using a cylindrical and plate surface area model. The pores considered for this analysis were the open pores in the fibers and not the ones opened by the mercury intrusion process. N_2 adsorption/desorption isotherm measurements were performed using an Autosorb-iQ gas sorption analyzer (Quantachrome Instruments) at 77 K. The Barrett−Joyner−Halenda (BJH) pore size distribution is estimated by the differential pore volume distribution (dV) versus the diameter of the pores (dD).[48] The S_{BET} was determined using the multi-point Brunauer−Emmett−Teller (BET) model, considering 11 equally spaced points in the P/P_0 range from 0.05 to 0.35, with P and P_0 being the N_2 pressure in the cell and the N_2 vapor pressure at the T of liquid N_2 (77 K), respectively. Prior to measurements, the samples were degassed for 3 h at 50 °C under vacuum to eliminate weakly adsorbed species. Of note that the method can reliably calculate a minimum pore size of 2 nm.

2.3.3. Chemical Characterization. The chemical composition and the possible chemical interactions of the components of the samples were studied with a fourier transform infrared (FTIR) spectrometer (Vertex 70v, Bruker), equipped with an attenuated total reflectance (ATR) accessory (MIRacle ATR, PIKE Technologies) using a diamond crystal. All spectra were recorded in the range of 4000−600 cm^{-1}, with a resolution of 4 cm^{-1}, accumulating 64 scans.

2.3.4. Thermal Properties. The thermal stability of the pure curcumin powder, pristine PCL fibers and curcumin-loaded PCL fibers was investigated by thermogravimetric analysis (TGA, Q500 system—TA Instruments). In particular, the samples were placed in aluminum pans and heated from 30 to 800 °C at a heating rate of 10 °C/min. The experiment took place in a N_2 atmosphere (flow rate, 50 mL/min).

The thermal behavior of the fibers was studied with the use of differential scanning calorimetry (Diamond DSC, PerkinElmer). Specifically, the pressed fibers in the form of pellets in sealed aluminum pans were heated from −90 to 250 °C under a dry N_2 purge. After keeping the samples at 250 °C for 1 min (isothermal), a cooling step down to −90 °C was performed and after 1 min at −90 °C, they were heated again up to 250 °C (all steps occurred at a rate of 10 °C/min). An empty pan was used as a reference cell. The instrument was calibrated with indium before use. The first heating cycle was performed in order to erase any aging events occurring during the storage of samples, whereas the second one was performed to determine the melting temperature (T_m). The first cooling cycle was performed to determine the crystallization temperature (T_c) of the samples.

Of note that in order to perform the TGA and DSC measurements, the fibrous materials had to be pressed into pellets. This was done by means of a CrusIR press (PIKE Technologies) with the use of 2t of weight.

2.3.5. Wetting Properties. The wetting properties of the mats were investigated by the static water contact angle, using a contact angle goniometer (OCAH-200, DataPhysics) at RT. A gas-tight 500 mL Hamilton precision syringe with a blunt needle of 0.52 mm internal diameter was used to deposit Milli-Q water droplets of 5 μL on the samples. Water contact angles were automatically calculated by the software. Ten droplets were deposited on each sample in different positions and then the average values were calculated.[49]

2.3.6. Tensile Testing. The mechanical properties of the porous fibrous mats were analyzed by performing stress−strain tests using a dual column tabletop universal testing System 3365, with 10 mm min^{-1} cross-head speed. Samples were cut in rectangular pieces with a width of 5 mm and an effective length of 25 mm. The Young's modulus, tensile strength, and elongation at break were calculated from the resulting stress−strain curves. An average value of five measurements is presented for each sample.[50]

2.4. Interaction of Curcumin with Off-Flavor Compounds. The interaction of curcumin powder with six different amines including the BAs CAD, PUT, and HIS and the volatile amines DMA, TMA, and ammonium hydroxide was investigated using a Cary 300 UV−visible spectrophotometer and a HORIBA Jobin Yvon Fluoromax-4 spectrofluorometer.[9] Specifically, a mother solution containing 0.0008% w/v curcumin in ethanol was prepared [named solution (1)]. Then, 0.1 mmol of each one of the amines was separately added in the polystyrene cuvettes that were containing 3 mL of the solution (1), and the UV−visible spectra were obtained. In order to take the fluorescence spectra, 0.1 mL of the solution (1) containing the amines was added in 2.9 mL of ethanol, to avoid the saturation of the spectra. Spectra were acquired in the range of 420−800 nm, with an excitation wavelength (λ_{exc}) of 425 nm, an excitation slit of 10 nm, and an emission slit of 5 nm.

2.4.1. CIELAB Color Space Analysis. For studying the colorimetric variation of the fibers, we used the CIELAB color space, a three-dimensional space designed for producing a color representation that mimics the human color perception. It consists of three components related to the lightness of the color (L), the hue position between red and green (a), and the hue position between yellow and blue (b). Given two CIELAB sample coordinates (L_1,a_1,b_1) and (L_2,a_2,b_2) describing the average color of the indicators extracted from different frames of videos or photos, their Euclidian distance (dE) provides an approximated quantitative measure of the human perceived color difference,[51] which can therefore be calculated using the following eq 1

$$dE = \sqrt{[(L_1 - L_2)^2 + (a_1 - a_2)^2 + (b_1 - b_2)^2]} \quad (1)$$

when d$E \geq 5$, the color difference is complete and clearly perceivable, whereas when it is d$E \geq 3.5$, the color difference can be noticed by inexperienced observers.[52]

The images of the mats have been acquired in RGB color coordinates using a reflex camera (Canon EOS 5D Mark II) and converted to CIELAB color coordinates in order to exploit the described space properties. During color conversion, the CIE standard illuminant D65 was used as a reference white point, theoretically corresponding to a color temperature of 6504 K.

2.4.2. Response Kinetics. The color evolution before, during and after exposure of the mats to DMA vapors was recorded using the reflex camera. Unless differently stated, all experiments were performed in a sealed homemade cell of volume ≈11 cm^3 equipped with two glass columns, where the mats (thickness, 0.020 ± 0.002 mm; dimensions, 1.0 cm × 0.5 cm; and weight, 0.58 ± 0.09 mg) were fixed (Figure S2 of Supporting Information). In there, 3 μL of ∼40% wt of a DMA aqueous solution droplet was placed through a tube which was sealed immediately after the droplet deposition. During the video acquisition, the DMA solution was inserted in the homemade cell containing the mat. A 4 min long video of 25 frames per second

https://doi.org/10.1021/acsapm.2c00418
ACS Appl. Polym. Mater. XXXX, XXX, XXX−XXX

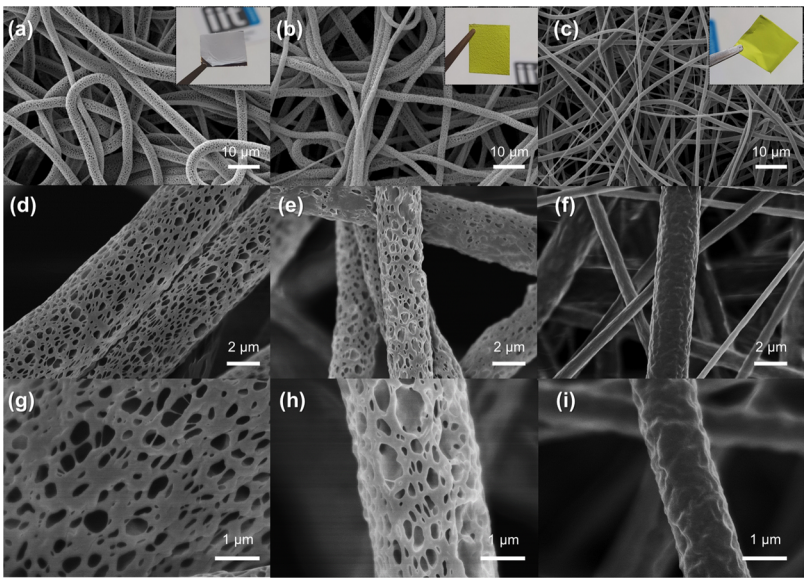

Figure 1. SEM analysis of the (a) pristine PCL, (b) PCLCU1, and (c) PCLCU1-NP mats. Insets: photos of the corresponding mats (sample size: approx. 1 cm × 1 cm). FE-SEM images of the (d,g) PCL, (e,h) PCLCU1, and (f,i) PCLCU1-NP fibers, at different magnifications.

was acquired, capturing the time before and during the exposure of the material to the DMA vapors inside the cell. Right after the 4 min and without stopping the video acquisition, the cell was opened and the video continued for 4 min more, in order to monitor the color recovery of the mats. The experiment was conducted in triplicates for the PCLCU1, PCLCU05, and PCLCU1-NP mats. It should be mentioned that, in all the cases involving video acquisition, the time point 0 s was defined at the time the droplet was inserted in the cell. All the videos were analyzed converting the relevant portion of the acquired images to CIELAB color coordinates and, subsequently, the Euclidian distance (dE) with respect to the color coordinate at time point 0 s has been plotted to graphs, showing the time evolution of the mean value of dE in each case. For the kinetics analysis, the abovementioned curves (dE vs t) were fitted using the pseudo-first-order kinetics as expressed in eq 2

$$dE = dE_{max} \times (1 - e^{(-k \times t)}) \quad (2)$$

where k is the reaction rate constant and t is in s.

2.4.3. Confocal Microscopy. The response kinetics of the PCLCU1 and PCLCU1-NP mats were also analyzed by spectrum live imaging, using a Nikon A1 confocal microscope (λ_{exc} = 561 nm, 20× objective). Each sample was fixed in the homemade cell and the DMA droplet was ejected in the system. The evolution of the fluorescence intensity at 604 nm was followed for a total time of 60 s (time point 0 s was defined at the time the droplet was inserted in the cell). The acquisition of the spectra was made by considering the fluorescence derived by the whole image of the sample part excited by the laser. The evolution of the fluorescence intensity was followed until it reached its maximum value.

2.4.4. Detection Limit. For the investigation of the color change behavior of the mats toward different concentrations of DMA, the samples were exposed to 10 different concentrations of DMA vapors in the cell ranging from 97.09 to 2.37 ppm. Specifically, droplets (3μl) of DMA aqueous solutions of various concentrations, adjusted in order to result to the abovementioned vapor concentrations, were inserted in the sealed homemade cell containing the sample. Subsequently, images were recorded every 30 s for 2 min monitoring the color change of the sample due to the formation of the DMA vapors in the cell. Then, the homemade cell was opened in order to provoke the release of the DMA vapors and to study the recovery of the sample's color to its initial condition. For all mats studied, the experiments were performed in triplicates and analyzed by converting the acquired images to CIELAB color coordinates.

2.4.5. Color Reversibility. For the investigation of the reversibility of the color of the mats after exposure to a specific amount of DMA vapors, 10 *yellow−red−yellow* cycles were performed. Specifically, at the time point 0 s, the DMA droplet solution was inserted in the sealed homemade cell containing the mat of interest. A 4 min long video of 25 frames per second was taken, capturing the time before and during the exposure of the material to the DMA vapors inside the cell. Right after the 4 min, the homemade cell was opened and images were acquired at the time points 15, 30, 60, 120, 180, and 240 s after the opening operation, in order to record the color recovery of the mats. This operation defines a full cycle, and was repeated for 10 times, in order to observe any variations in the color and the response time along the cycles. The videos and images were analyzed with CIELAB color space analysis, and the dE values were calculated as follows: (i) the color difference between the CIELAB sample coordinates at the end of the previous cycle and after the amine exposure (dE_max) in order to explore if the color shift underwent by the mat in each cycle is perceivable by a human observer and (ii) the color difference between the CIELAB sample coordinates of the mat before any exposure and the CIELAB sample coordinates at the end of each cycle (dE_min). To explore if the capability of the mat to modify its color when interacting with the amine vapors changes cycle after cycle, the color difference between the original CIELAB sample coordinates of the mat and the CIELAB sample coordinates after the amine exposure of each cycle was also measured (dE_max$_2$). The fitting of the kinetics derived from the CIELAB analysis (dE vs t) of the "yellow to red" part of the cycles was constructed by using eq 2, in order to observe possible changes in the reaction rate k during the cycles. The experiment was conducted in triplicates.

3. RESULTS AND DISCUSSION

For the fabrication of the porous fibers, the non-solvent-induced phase separation mechanism was adopted. Specifically, the presence of the non-solvent in the PCL solution creates thermodynamic instability and induces the phase separation into a polymer-rich and a polymer-poor phase.[43] During electrospinning, the non-solvent, mainly concentrated in the polymer-poor phase, evaporates last due to its higher boiling point, leaving behind a porous morphology within the polymer fibers.[47] Following this approach, electrospun mats in the form of homogeneous paper-like films are formed, white in the case of pure PCL and yellow, representative of the curcumin dye

https://doi.org/10.1021/acsapm.2c00418
ACS Appl. Polym. Mater. XXXX, XXX, XXX−XXX

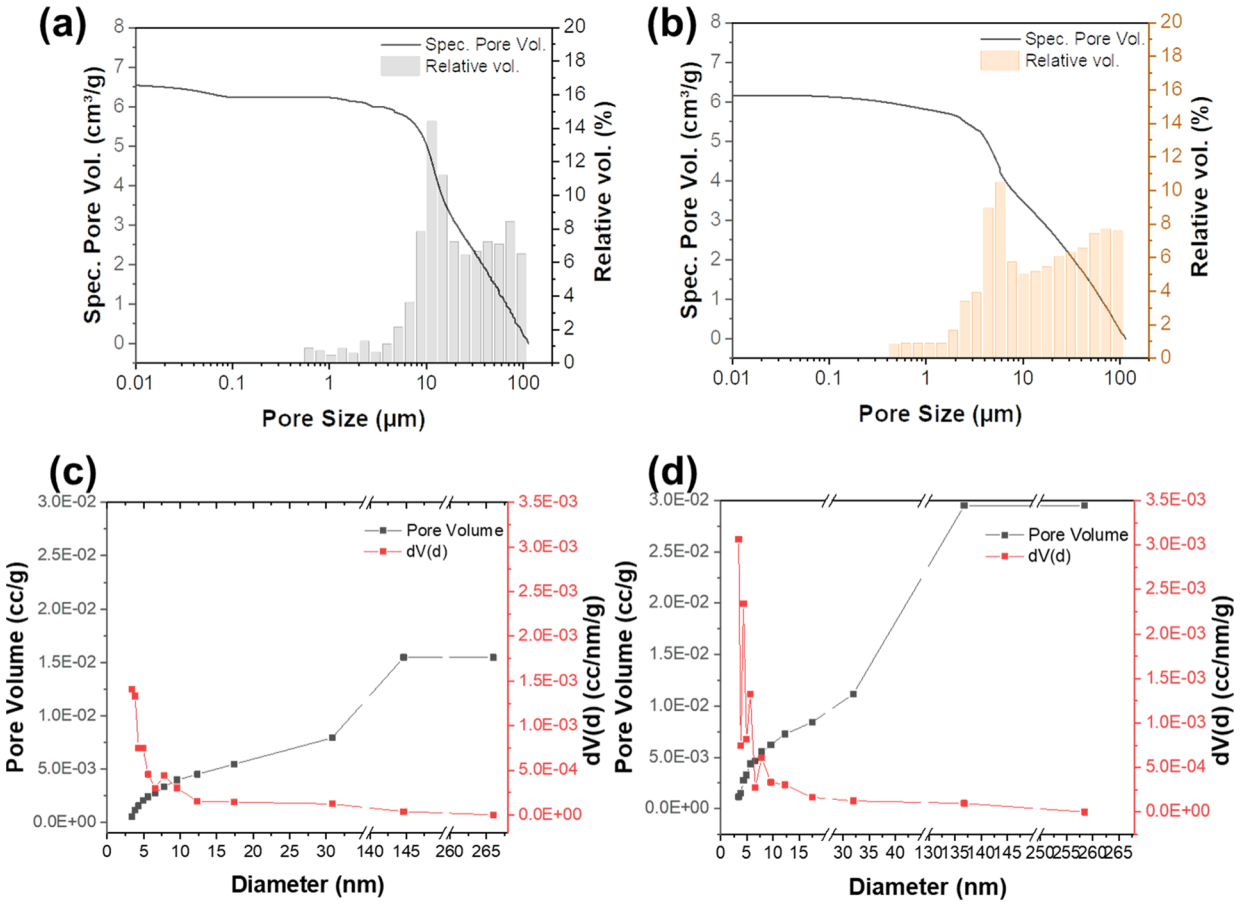

Figure 2. Pore size distribution in the macropore range of the (a) PCL and (b) PCLCU1 mats obtained from MIP. BJH pore size distribution in the mesopore range of the (c) PCL and (d) PCLCU1 mats obtained by N_2 physisorption.

color, in the PCLCU1 case (insets of Figure 1a,b). A closer look with SEM analysis indicates that the mats present irregularly shaped interconnected interfibrillar pores in the range of a few tens of μm, and they consist of a net of randomly distributed defect-free polymeric fibers with an average diameter 3.81 ± 1.60 μm and 2.88 ± 0.87 μm for the PCL and PCLCU1 mats, respectively (size distribution analysis Supporting Information Figure S3a,b). Most importantly, a closer look of the fibers with FE-SEM demonstrates the presence of well-defined intrafibrillar pores, distributed homogeneously throughout the surface of the individual fibers, with their majority in the sub-micrometric size range, between few hundreds and few tens of nm (Figure 1d,e,g,h). Mats with lower amount of curcumin in the PCL fibers (PCLCU05) present no significant difference in the size and morphology (Figure S4a,b, Supporting Information), whereas the non-porous PCLCU1-NP fibers have an embossed, pore-less surface, and present an average diameter of 1.85 ± 0.68 μm, slightly smaller than the porous ones (Figure 1c,f,i).

As it can be noted in SEM images of Figure S5a,b, the fibers were able to maintain their porous structure even after their compression with 2t of weight. The stability of the porous structure was also confirmed by the morphological examination of the mats after being subjected to the mechanical stress−strain tests, where it can be noted that the porous structure is perfectly maintained (Figure S5c,d, Supporting Information). It should be also mentioned that the mechanical test analysis proved that the presence of curcumin slightly affects the mechanical properties of the PCL mats (Figure S6, Supporting Information and Note S1).

In order to have a detailed insight into the porous structure of the electrospun mats, MIP and BET N_2 adsorption/desorption isotherm analyses were performed (Figure 2). In particular, MIP was used to analyze the characteristics of the macropores (interfibrillar and intrafibrillar pores, see FE-SEM Figure 1d,e), whereas BET allowed the investigation of the porous structures in the nanometric size range (mesoporous intrafibrillar structure, see FE-SEM, Figure 1g,h).

As shown in the intrusion and extrusion isotherms derived from the MIP measurements (Figure S7, Supporting Information), in all samples the presence of interconnected pore structures is confirmed by the large volume of mercury entrapped in the fibrous mats after the extrusion. Both the unloaded and loaded with curcumin mats present macropores with a size range between 0.7 and 120.0 μm. The submicrometric pores can be likely attributed to the intrafibrillar pores (on/in the individual fibers), whereas the bigger pores to the interfibrillar space of the mats. The prevalent pore size range of the pristine PCL mat is between 10.05 and 17.10 μm (Figure 2a), whereas for the PCLCU1 mat is between 3.84 and 6.72 μm (Figure 2b), possibly because the fibers of the curcumin-loaded mat are smaller, as noticed from SEM image analysis, favoring their closer interfibrillar arrangement. Nonetheless, the effective porosity of all the porous fiber mats studied is similar and ca. 88% (88.74% for the pristine PCL mat and 88.42% for the PCLUCU1 mat) and slightly higher than the non-porous fiber mat (PCLCU1-NP, 85.80%),

https://doi.org/10.1021/acsapm.2c00418
ACS Appl. Polym. Mater. XXXX, XXX, XXX−XXX

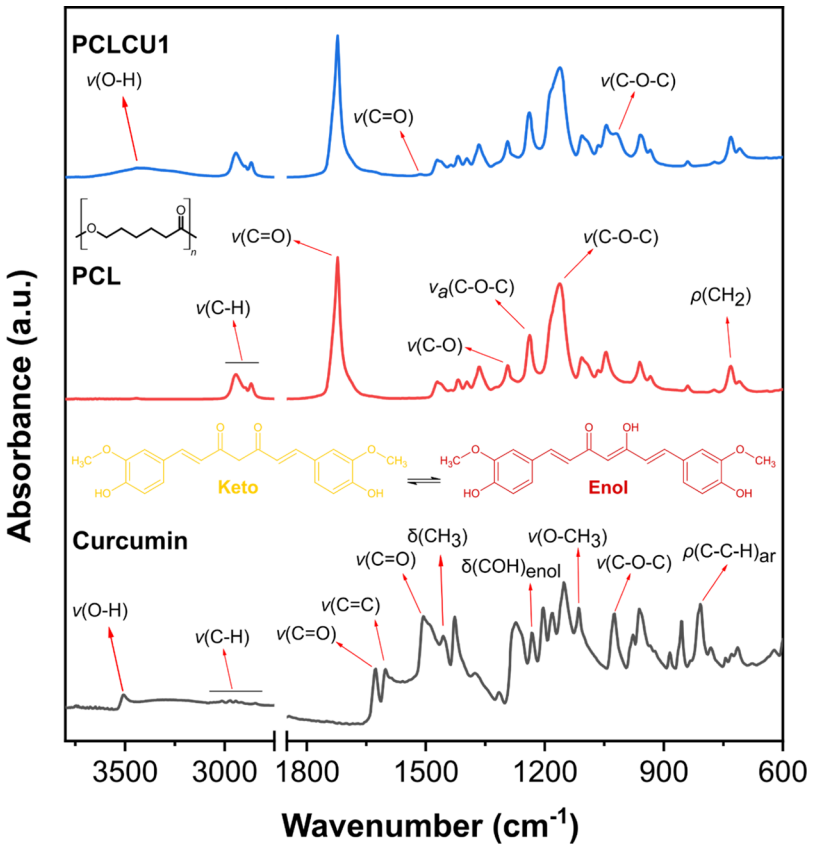

Figure 3. ATR-FTIR spectra of curcumin powder, PCL, and PCLCU1 mats.

demonstrating that the porous fibers slightly enhance the overall porosity of the mats, whereas the presence of curcumin does not significantly affect their overall structural parameters.

As for the nanometric pores, the type IV isotherms derived from the BET study (Figure S8, Supporting Information) suggest that the developed mats belong to the mesoporous (2−50 nm) and macroporous (>50 nm) materials, according to the IUPAC recommendation.[53] As revealed by the comparison of Figure 2c,d, the presence of curcumin affects the overall pore size and the total pore volume in the nanometric range. In fact, the pore volume (V_P) is almost double in the case of PCLCU1 (0.030 $cm^3\ g^{-1}$, Figure 2d) compared to the PCL porous fiber mat (0.015 $cm^3\ g^{-1}$, Figure 2c), indicating that there are more pores available for the N_2 adsorption in the former case. The effect of the curcumin in the mesoporosity can be further supported by the comparison with the PCLCU05 mat (Figure S4d of Supporting Information), where it is visible that the lower amount of curcumin results in the formation of pores in the nanometric range that are more than the ones of the pure PCL mat and less than the ones of PCLCU1 mat, presenting an intermediate condition. Most importantly, the presence of curcumin leads also to a gradual increase of the S_{BET} of the porous samples, from 6.1 $m^2\ g^{-1}$ for the pristine PCL, to 7.9 $m^2\ g^{-1}$ for the PCLCU05, and to 8.1 $m^2\ g^{-1}$ for the PCLCU1 mats.

A similar study on the PCLCU1-NP shows the existence of a very small number of nanosized pores with a main pore size of ca. 3.4 nm, possibly attributed to the intrinsic porosity of the fibers due to the polymer chain configuration in the presence of curcumin and not to the pores formed by the non-solvent-induced phase separation process (Figure S9, Supporting Information), whereas as expected, the V_P is significantly higher in the case of the porous (0.030 $cm^3\ g^{-1}$, Figure 2d) compared to the non-porous curcumin-loaded fiber mats (0.010 $cm^3\ g^{-1}$, the 33.3% of PCLCU1, Figure S10). By analyzing the S_{BET} of the mats, a considerable difference between the porous and non-porous mats is also revealed. Specifically, as shown in Figure S10, the S_{BET} of the PCLCU1-NP mats is 4.3 $m^2\ g^{-1}$, almost 50% of the one of the porous counterpart (8.1 $m^2\ g^{-1}$).

The chemical properties of the samples and their components were studied by ATR-FTIR spectroscopy and are presented in Figure 3. The spectrum of curcumin is a complex overlap of signals attributed to several conformations and orientations of the molecule.[54] Indeed, curcumin is presented simultaneously in enol and keto forms due to tautomeric resonance, with the spectrum showing the typical bands of the two states, as it can be noticed in Table S1 of Supporting Information.[55] The ATR-FTIR spectrum of PCL shows the characteristic absorptions of the polymer.[56] In the case of the PCLCU1 mat, the ATR-FTIR spectrum shows all the characteristic peaks of the PCL polymeric structure, whereas some peaks representative of the curcumin can also be identified in the areas with no spectral overlap. In particular, the C═O stretching mode of curcumin appears shifted to 1514 cm^{-1} (1506 cm^{-1} in the pure curcumin). This is also the case for the C−O−C stretching mode which is observed at 1018 cm^{-1} instead of 1024 cm^{-1}. Furthermore, a band representative of the O−H stretching appears at 3431 cm^{-1}. Although in the curcumin spectrum, the narrow O−H stretching at 3509 cm^{-1} represents the typical O−H free from intermolecular interactions, in the PCLCU1 sample, the

https://doi.org/10.1021/acsapm.2c00418
ACS Appl. Polym. Mater. XXXX, XXX, XXX−XXX

O−H shifted to lower wavenumbers is also broadened, suggesting the formation of H-bonds. All these changes suggest a different conformation of curcumin once inside the polymeric structure, with H-bonds well established.

The thermal stability and behavior of the mats were studied by TGA and DSC analysis. As noted in TGA analysis of Figure S11a,b of Supporting Information, the presence of curcumin did not affect the thermal degradation of the fibers, which was representative of the PCL polymer. The DSC thermograms (Figure S11c, Supporting Information) further confirm that the presence of curcumin in the PCL matrix does not significantly affect the thermal behavior of the polymer. Specifically, the glass transition temperature (T_g) and the melting point (T_m) of all the studied mats can be noted at −63 and 55 °C, respectively, and these are the representative values of the pure PCL mat. This is also the case for the wetting properties of the developed mats. Both PCLCU05 and PCLCU1 mats are hydrophobic systems, with a water contact angle of 138.6 ± 4.9° and 135.7 ± 4.0°, respectively (Table S2, Supporting Information), which are not significantly different from the pure PCL mats (135.3 ± 3.7°).

As already mentioned, curcumin has the property of changing its chemical conformation in environments of different acidity, and this results in a different color of the molecule.[57] Based on the fact that off-flavor compounds such as amine-based molecules are able to increase the pH of the environment due to their alkaline nature,[58] the color behavior of curcumin when in contact with different amines in solution was first studied. Specifically, curcumin powder was exposed to ethanol solutions containing CAD, PUT, HIS, DMA, TMA, and ammonium hydroxide. As clearly noticed in Figure 4, the

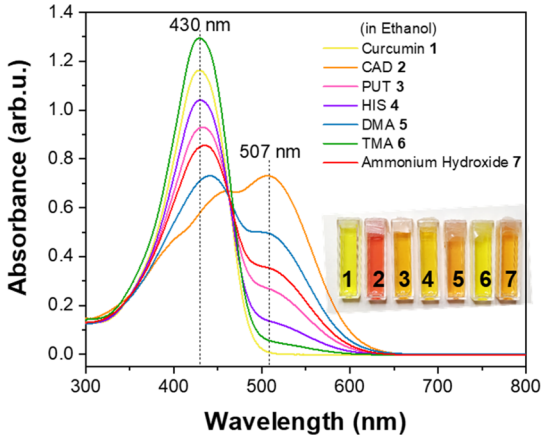

Figure 4. Absorption spectrum of pure curcumin in ethanol and of curcumin in ethanol in the presence of off-flavor compounds. In the inset is presented the photograph of the corresponding solutions: (1) curcumin in ethanol, and curcumin in ethanol with (2) CAD, (3) PUT, (4) HIS, (5) DMA, (6) TMA, and (7) ammonium hydroxide.

curcumin solution changes color when the different off-flavor compounds are present, with hues from dark yellow to red, depending on the amine compound to which it is exposed. The difference in the color can be also noticed spectroscopically in the UV−visible range. In particular, the enolate double bond that is formed in the presence of the amine compounds extends the conjugation system of curcumin's structure,[9,59] resulting in a new absorption peak at 507 nm. At the same time, a decrease of the intensity of the representative peak of curcumin at 430 nm can be noted—typical for curcumin dissolved in organic solvents and likely assigned to the low energy $\pi-\pi^*$ transition of curcumin's carbonyl groups[9,59−61]—which also presents a slight bathochromic shift (Figure 4), probably due to the distortions of the molecule's chromophore.[62] The difference in the color change depends on the pH increase induced by each amine to the initial solution, which can be different because amines present a broad pK_a range.[63] Additionally, the fluorescence intensity of the keto form of curcumin that normally appears at 534 nm (upon excitation at 425 nm), falls, and such quenching is notable in Figure S12 of Supporting Information.

However, in real-life cases such as the one of spoiled food (e.g., fish, meat, etc.), off-flavor compounds are released from the food and some of them gradually take the form of vapors, modifying the packaging atmosphere.[64] Therefore, for food packaging applications, the colorimetric indicator may not be in direct contact with the food, but can be included in the headspace of the packaging and thus be exposed to its atmosphere.[65] Hence, and as highlighted in the introduction, the need to address the response of such indicators in the presence of these compounds in the form of vapors[66] and not of liquids is essential for verifying their accuracy and their realistic applicability to food packaging systems.[9]

To investigate the responsiveness of the fibers toward amines, a kinetics study on the color evolution of the PCLCU1 mats upon exposure to DMA vapors was conducted. The porous material was exposed to DMA vapors (97.09 ppm) that were generated by the evaporation of a 3 μL-droplet of DMA aqueous solution. As shown in Figure 5a, the CIELAB color space analysis shows that the color of the mats evolves rapidly over time when exposed to these vapors from yellow to red. As the dE values demonstrate, a complete color change occurs after 5.1 ± 1.3 s (d$E \geq 5$), surpassing the limit of visual perception for inexperienced users after 4.7 ± 1.3 s (d$E \geq 3.5$). The material reaches a maximum dE value of 56.0 ± 2.2 after 107.1 ± 24.7 s (Figure 5a).

The effect of the fibers' pores on the responsivity of the material is evaluated upon exposing to the same concentration of DMA vapors the non-porous PCLCU1-NP mats (Figure 5b). As the CIELAB color space analysis showed, PCLCU1-NP reached a maximum dE value smaller than in the case of the porous fibers, 32.4 ± 1.4 in 103.8 ± 1.0 s, whereas it reached the aforementioned dE values of 3.5 and 5 in a time of 3.7 ± 0.9 s and 5.16 ± 1.0 s, respectively (Figure 5b). In a more detailed comparison between the PCLCU1 and the PCLCU1-NP mats, and in order to prove the importance of the pores on the responsivity of this type of mats, the kinetics study was performed through the fitting with the pseudo-first-order kinetics model (eq 2) in both cases.

By analyzing the rate k, the difference in the kinetics behavior of the porous and the non-porous fibers can be confirmed. Specifically, PCLCU1 presents a k of (95.2 ± 0.8) × 10^{-3} s^{-1}, whereas the PCLCU1-NP mats have a k of (65.3 ± 0.3) × 10^{-3} s^{-1}, implying that the reaction of the porous fibers with the DMA vapors is faster than the one of the non-porous ones. Indeed, although the maximum dE value for the porous PCLCU1 (56.0 ± 2.2) is reached in a relatively longer time than the one of the non-porous PCLCU1-NP, the PCLCU1 reaches the maximum dE value of the PCLCU1-NP mat (32.4 ± 1.4) in just 11.3 ± 2.4 s. This information, along with the fact that the porous fibers reach a much higher dE maximum value than the non-porous ones (56.0 ± 2.2 > 32.4 ± 1.4), confirms the claim that the highly porous structure is more

https://doi.org/10.1021/acsapm.2c00418
ACS Appl. Polym. Mater. XXXX, XXX, XXX−XXX

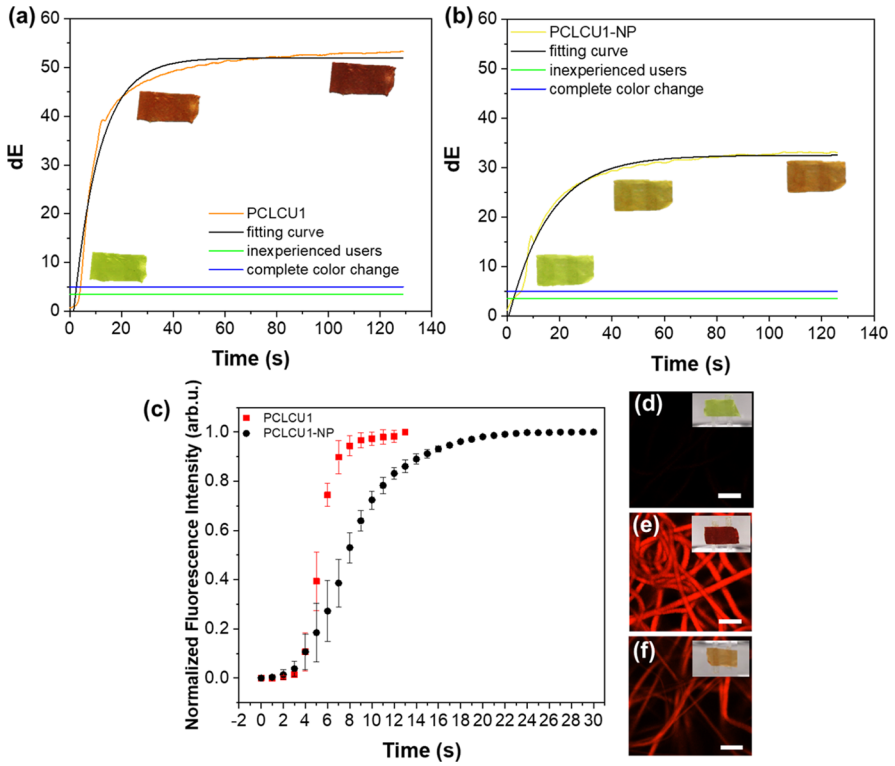

Figure 5. CIELAB color space analysis kinetics curves of the color of (a) PCLCU1 and (b) PCLCU1-NP mats upon exposure to DMA vapors with their corresponding fitting curves, and in the insets the images before and during the exposure until the maximum d*E*. (c) Time needed for the PCLCU1 and PCLCU1-NP mats to reach their maximum fluorescence intensity at ~604 nm (λ_{exc} = 561 nm) upon exposure to DMA vapors. (d) Mats before exposure to DMA and (e) PCLCU1 and (f) PCLCU1-NP during exposure to DMA. Confocal image scale bar = 10 μm and sample size = 1.0 cm × 0.5 cm.

effective for the tracing of DMA and thus for the use as an indicator. As previously mentioned, the surface area of the PCLCU1 mat is much higher than the one of the PCLCU1-NP mat. For this reason, more surface of the PCLCU1 is exposed to the atmosphere, and subsequently, more curcumin is directly available to react with the amine vapors. This also explains the fact that PCLCU1 needs more time to reach its maximum d*E* value in comparison with PCLCU1-NP because the more the available curcumin to react with the DMA vapors, the more the time the material needs for the complete interaction. The latter can also be supported by the recovery of the mats to the yellow color after their exposure to the DMA vapors. As shown in Figure S13 of Supporting Information, both PCLCU1 and PCLCU1-NP mats were able to return to their yellow color in 41.4 ± 10.0 s and 25.8 ± 2.7 s, respectively, indicating that the PCLCU1-NP returns much faster than the PCLCU1, most likely because there may be a partial interaction of DMA with the curcumin and as a result a limited transition of the pigment to its enolate form.

Of note, all aforementioned results can be further verified by the fact that same experiments on the PCLCU05 show a better ability to reach high d*E* values (45.2 ± 1.7 in 95.6 ± 14.3 s, see Figure S14, Supporting Information) compared to the PCLCU1-NP mat, even though it contains half of the curcumin.

The interaction of the DMA vapors with the PCLCU1 and PCLCU1-NP mats was also evaluated by confocal kinetic studies, and more specifically, by following the evolution of the fluorescence intensity upon exposure to DMA vapors over time. Depending on the molecular environment, curcumin presents a different photochemical behavior and thus fluorescent properties.[67] As referred before, when the keto form predominates, we can see a fluorescence peak at 534 nm upon excitation at 425 nm, whereas in its enol form, the quenching of this peak is noticed (Figure S12, Supporting Information). In the enol form, a new absorption peak arises at 507 nm, and correspondingly, upon excitation of this peak (λ_{exc} = 561 nm), a fluorescence peak is formed at around 604 nm, as shown in Figure S15. Hence, in order to measure the interaction with DMA, the fluorescence of the enol form was examined. From Figure 5c, it is notable that the modification of the fluorescence intensity of the porous fibers is faster than the one of the non-porous ones, and the rate of the fluorescence growth is three times faster (Supporting Information Note S2 and Figure S16). This is proof that when in contact with the DMA vapors, the curcumin contained in the PCLCU1 mats reacts by changing to the enol form much faster compared to the PCLCU1-NP mats.

The response of the fibers and the change in their color and fluorescence can be noted in Figure 5d–f; before the exposure to DMA vapors, the fibers present their initial yellow color and no fluorescence is observed in the captured confocal microscope image (Figure 5d). As soon as the mats are exposed to the vapors, the color of the fibers changes, and they become fluorescent with more intense modifications in the case of the porous fiber mats (Figure 5e,f). This can be attributed to the fact that the PCLCU1 mat has a higher surface area and therefore more curcumin molecules interact with the DMA vapors, turning from the keto to the enol form, compared to the PCLCU1-NP.

Once the color change upon exposure to DMA vapors by the kinetics study for both porous and non-porous mats is

https://doi.org/10.1021/acsapm.2c00418
ACS Appl. Polym. Mater. XXXX, XXX, XXX−XXX

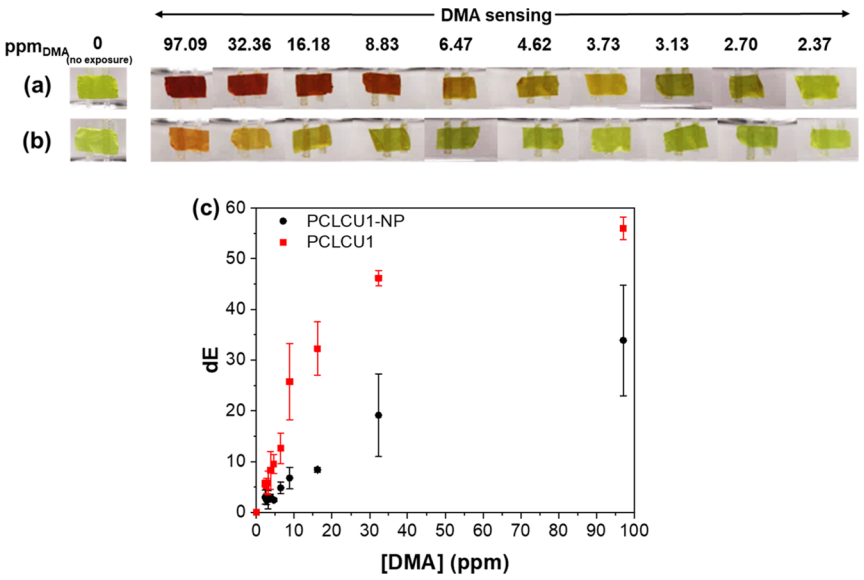

Figure 6. (a) PCLCU1 and (b) PCLCU1-NP mats before and during their exposure to DMA vapors of different concentrations. (c) Maximum d*E* values that the PCLCU1 and PCLCU1-NP mats reach upon exposure to different concentrations of DMA vapors.

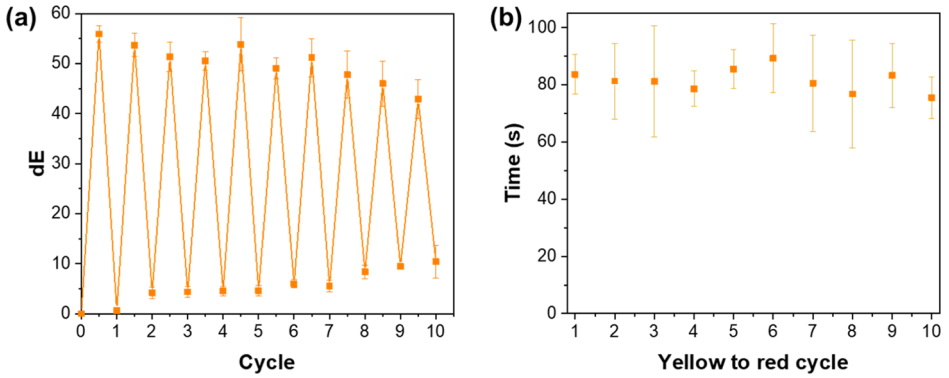

Figure 7. Modification of the d*E* value of the PCLCU1 mat upon cyclic exposure to DMA vapors. Each cycle consists of exposure to DMA vapors (97.09 ppm) and subsequent exposure to atmospheric conditions. For each cycle, the d*E*_max value is measured by considering the CIELAB color coordinates of the sample after DMA exposure and at the end of the previous cycle, and the d*E*_min values derive from the CIELAB color coordinates of the sample after exposure to atmospheric conditions and the CIELAB color coordinates of the sample before any exposure. (b) Time needed for the PCLCU1 mats to reach the maximum d*E* value for each exposure cycle.

confirmed, the investigation of their color change behavior toward various concentrations of the DMA was performed. In other words, the estimation of the lowest DMA quantity that can be traced by the indicators through visually perceivable color changes was studied. Specifically, in Figure 6a,b, it is shown that the PCLCU1 mat presents a more intense color change than its non-porous equivalent, visible by inexperienced users even in the presence of just 2.37 ppm of DMA vapors (Figure 6a,c), in contrary to the PCLCU1-NP that presents an evident color change starting from a minimum concentration of 8.83 ppm (Figure 6b,c). The PCLCU1 presents a d$E \geq 5$ for all of the DMA concentrations studied, ranging from 97.09 to 2.37 ppm (Figure 6c), demonstrating that the developed material is very sensitive toward the herein studied amine. On the other hand, the d*E* value of the PCLCU1-NP mat falls below 5 for DMA concentrations lower than 8.83 ppm, whereas it also presents values ≤ 3.5, thus making the color change perception difficult for inexperienced users.

Focusing on the low DMA concentrations, a linear dependence with the d*E* value is observed (Figures 6c and S17), indicating a direct interaction of the curcumin molecules with the DMA vapors switching to the enol form. At higher DMA concentrations a color saturation is reached, designating that most of the curcumin molecules have reached their enol form at lower DMA concentrations. From the linear fitting analysis of the data at the low-concentration range (Note S3, Supporting Information), the concentration of DMA at which the d*E* value surpasses the limit of 5 is found, which is 2.33 and 9.26 ppm for the PCLCU1 and PCLCU1-NP mats, respectively, confirming the estimations done by using the CIELAB color space analysis. Thus, it can be verified that the PCLCU1-NP mats present an incapability to respond adequately to DMA vapor concentrations lower than ca. 9 ppm, attributed to their lower available surface area and thus to the limited interaction with the DMA vapors.

In order to evaluate the indicator's ability to be reutilized, the reversibility and reusability of the PCLCU1 mats was studied for 10 cycles of exposure to 97.09 ppm of DMA vapors and subsequent exposure to the atmospheric conditions. In Figure 7a, it can be noted that after exposing the material to DMA vapors, its color changes significantly (d$E = 55.9 \pm 1.6$), becoming red, due to the predominant enol form of curcumin.

https://doi.org/10.1021/acsapm.2c00418
ACS Appl. Polym. Mater. XXXX, XXX, XXX−XXX

The subsequent opening of the gas chamber leads to the release of the DMA vapors and thus to the exposure of the indicator to normal atmospheric conditions. This results in the gradual reversion of curcumin to its keto form,[68] and, as a result, to the reduction of the color difference with respect to the original yellow color of the material (final $dE = 0.6 \pm 0.1$). As already mentioned above, this *yellow-red-yellow* color change is always complete ($dE > 5$) and visually perceivable by inexperienced users ($dE > 3.5$), whereas it is repeatable for at least 10 consecutive DMA vapor exposure−release cycles. As shown in Figure 7a, in each cycle, not all of the curcumin molecules return from the enol to their keto form, indicating a slight change of the starting color of the material, but the color change is always intense, with $dE > 42$ with respect to the starting color of each cycle, and with $dE > 50$ with respect to the original color (Figure S18, Supporting Information). The time needed to reach the dE_max value is slightly altered from cycle to cycle, too (Figure 7b) without affecting the overall efficacy of the material to detect the changes in the atmosphere because the response time—the time needed to acquire easily perceivable dE values—was always in the range of 76.8 ± 18.8−89.3 ± 12.0 s. This can be also confirmed by the kinetics rate constant extracted by eq 1, with the k value to be always between $(97.9 \pm 0.5) \times 10^{-3}$ s^{-1} (cycle 4) and $(77.6 \pm 0.3) \times 10^{-3}$ s^{-1} (cycle 6) (Table S3, Supporting Information). Hence, the rate of the reaction of curcumin to DMA vapors is not affected significantly by the repeated DMA exposure, confirming that the developed material is a colorimetric indicator that can be effectively reused for at least 10 cycles.

The presented study reveals the importance of the highly porous structure for an effective and real-time colorimetric indication of alkaline vapors. Compared to the majority of the studies presented so far on colorimetric indicators containing natural molecules[24,25,69] such as curcumin,[9,15,19−23,25,26,28−30] which test the efficiency of the material to change color in the presence of buffer solutions,[20,30,33] acidic or alkaline vapors,[19,23,26,29,34] and/or acidic or alkaline semisolid media[19] without proper investigation of different concentrations, or with no precise evaluation of the kinetics of the color change and reusability,[15,19] this work offers a comprehensive view of the overall performance of the system in terms of responsivity, sensitivity, and reusability. Compared to the already explored curcumin-based films[15,19−23,26] and fibrous mats,[9,25,28] but also compared to other types of colorimetric indicators,[26,30] PCLCU1 mats present faster color change response and higher sensitivity. This performance occurs using very thin and light membranes containing very low amounts of curcumin. Following this approach, studies on the performance in more complex environments could pave the way for an alternative type of colorimetric indicators that are able to rapidly indicate the presence of alkaline vapors, utilized multiple times even in a domestic environment by the end users.

CONCLUSIONS

In this study, reversible colorimetric highly porous indicators were fabricated upon the combination of biodegradable and natural materials, namely, PCL and curcumin. The SEM, BET, and MIP analysis confirmed the high porosity of the material, which results in a significant responsiveness to DMA vapors, even in the presence of minor concentrations in the studied environment. The color changes of the porous material can be visually perceived even by inexperienced users, as demonstrated by CIELAB color space analysis. Above all, results showed that the porous fiber mats present an increased sensitivity compared to their non-porous equivalents and, consequently, to the vast majority of the up to date colorimetric indicators, which have mostly the form of films[15,19−25] or pore-less fibers.[9,25,28] The presented study highlights the importance of the high porosity for an efficient and rapid visual inspection of the alkaline environment, necessary for various applications, such as intelligent food packaging, environmental protection, and biomedicine.

ASSOCIATED CONTENT

Supporting Information

The Supporting Information is available free of charge at https://pubs.acs.org/doi/10.1021/acsapm.2c00418.

Chemical structures of curcumin; experimental setup; size distribution of the fibers; characterization of the PCLCU05 mats; characterization of the PCLCU1-NP mats; morphology of the compressed and stressed fibers; mechanical characterization; MIP and BET characterization; ATR-FTIR analysis; TGA and DSC analysis; water contact angle analysis; fluorescence spectra of curcumin in the presence of off-flavor compounds; color changes of the amine-exposed mats; color changes of PCLCU05 mats in the presence of DMA vapors; fluorescence evolution of the enol form of the mats in the presence of DMA vapors; fitting analysis of the fluorescence evolution over time of the mats; fitting analysis of the dependence of the maximum dE value to the DMA concentration; color reversibility of the PCLCU1 mats for 10 cycles; and reaction rate constants for 10 cycles (PDF)

AUTHOR INFORMATION

Corresponding Author

Despina Fragouli − *Smart Materials, Istituto Italiano di Tecnologia, 16163 Genova, Italy;* orcid.org/0000-0002-2492-5134; Email: despina.fragouli@iit.it

Authors

Despoina Kossyvaki − *Smart Materials, Istituto Italiano di Tecnologia, 16163 Genova, Italy; Dipartimento di Informatica Bioingegneria, Robotica e Ingegneria dei Sistemi (DIBRIS), Università degli studi di Genova, 16145 Genova, Italy;* orcid.org/0000-0002-8315-611X

Aurelio Barbetta − *Smart Materials, Istituto Italiano di Tecnologia, 16163 Genova, Italy*

Marco Contardi − *Smart Materials, Istituto Italiano di Tecnologia, 16163 Genova, Italy*

Matteo Bustreo − *Pattern Analysis and Computer Vision, Istituto Italiano di Tecnologia, 16152 Genova, Italy*

Katarzyna Dziza − *Smart Materials, Istituto Italiano di Tecnologia, 16163 Genova, Italy; Dipartimento di Informatica Bioingegneria, Robotica e Ingegneria dei Sistemi (DIBRIS), Università degli studi di Genova, 16145 Genova, Italy;* orcid.org/0000-0002-1237-665X

Simone Lauciello − *Electron Microscopy Facility, Istituto Italiano di Tecnologia, 16163 Genova, Italy*

Athanassia Athanassiou − *Smart Materials, Istituto Italiano di Tecnologia, 16163 Genova, Italy;* orcid.org/0000-0002-6533-3231

Complete contact information is available at:

https://doi.org/10.1021/acsapm.2c00418
ACS Appl. Polym. Mater. XXXX, XXX, XXX−XXX

https://pubs.acs.org/10.1021/acsapm.2c00418

Author Contributions

The manuscript was written through contributions of all authors. All authors have given approval to the final version of the manuscript.

Notes

The authors declare no competing financial interest.

■ ACKNOWLEDGMENTS

The authors would like to thank Giorgio Mancini (Smart Materials, IIT) for density and MIP analysis, Lara Marini (Smart Materials, IIT) for TGA and DSC analysis, Mirko Prato and Lea Pasquale (Materials Characterization Facility, IIT) for BET analysis, Marco Scotto (Nanoscopy & NIC, IIT) for the fruitful discussions on confocal microscopy, Lìa Vàsquez (Smart Materials, IIT) for her help with the MIP data elaboration, Arkadiusz Zych (Smart Materials, IIT) and Sergey Artyukhin (Quantum Materials Theory, IIT) for the useful discussions, and Abdulaziz Abubshait (Social Cognition in Human−Robot Interaction, IIT) for English editing.

■ REFERENCES

(1) Nout, M. J. R. Food Technologies: Fermentation. *Encyclopedia of Food Safety*; Academic Press, 2014; Vol. 3, pp 168−177.
(2) Biji, K. B.; Ravishankar, C. N.; Venkateswarlu, R.; Mohan, C. O.; Gopal, T. K. S. Biogenic Amines in Seafood: A Review. *J. Food Sci. Technol.* **2016**, *53*, 2210−2218.
(3) Mathias, K. S. Identifying and Preventing Off-Flavors. https://www.ift.org/news-and-publications/food-technology-magazine/issues/2004/november/features/identifying-and-preventing-off-flavors (accessed Feb 28, 2022).
(4) Yang, X.; Zhang, J.; Cheng, Y. The Evaluation of the Three Edible Tissues of Dead Adult Chinese Mitten Crabs (Eriocheir Sinensis) Freshness in Harvest Season, Based on the Analysis of TVBN and Biogenic Amine. *SpringerPlus* **2016**, *5*, 1906.
(5) Ladero, V.; Calles-Enriquez, M.; Fernandez, M.; Alvarez, M. Toxicological Effects of Dietary Biogenic Amines. *Curr. Nutr. Food Sci.* **2010**, *6*, 145−156.
(6) Meng, Y.; Luo, H.; Dong, C.; Zhang, C.; He, Z.; Long, Z.; Cha, R. Hydroxypropyl Guar/Cellulose Nanocrystal Film with Ionic Liquid and Anthocyanin for Real-Time and Visual Detection of NH3. *ACS Sustain. Chem. Eng.* **2020**, *8*, 9731−9741.
(7) Huis In't Veld, J. H. J. H. Microbial and Biochemical Spoilage of Foods: An Overview. *Int. J. Food Microbiol.* **1996**, *33*, 1−18.
(8) Genovese, M. E.; Zia, J.; Fragouli, D. Natural and Biocompatible Optical Indicators for Food Spoilage Detection. *Sustainable Food Packaging Technology*; John Wiley & Sons, 2021; pp 369−393.
(9) Luo, X.; Lim, L.-T. Curcumin-Loaded Electrospun Nonwoven as a Colorimetric Indicator for Volatile Amines. *Lwt* **2020**, *128*, 109493.
(10) Aghaei, Z.; Emadzadeh, B.; Ghorani, B.; Kadkhodaee, R. Cellulose Acetate Nanofibres Containing Alizarin as a Halochromic Sensor for the Qualitative Assessment of Rainbow Trout Fish Spoilage. *Food Bioprocess Technol.* **2018**, *11*, 1087−1095.
(11) Liang, T.; Wang, L. A PH-Sensing Film from Tamarind Seed Polysaccharide with Litmus Lichen Extract as an Indicator. *Polymers* **2017**, *10*, 13.
(12) Dong, H.; Ling, Z.; Zhang, X.; Zhang, X.; Ramaswamy, S.; Xu, F. Smart Colorimetric Sensing Films with High Mechanical Strength and Hydrophobic Properties for Visual Monitoring of Shrimp and Pork Freshness. *Sens. Actuators, B* **2020**, *309*, 127752.
(13) Kuntzler, S. G.; Costa, J. A. V.; Brizio, A. P. D. R.; Morais, M. G. d. Development of a Colorimetric PH Indicator Using Nanofibers Containing Spirulina Sp. LEB 18. *Food Chem.* **2020**, *328*, 126768.
(14) Kumavat, S. D.; Chaudhari, Y. S.; Borole, P.; Mishra, P.; Shenghani, K.; Duvvuri, P. Degradation Studies of Curcumin. *Int. J. Pharm. Rev. Res.* **2013**, *3*, 50−55.
(15) Chen, H.-z.; Zhang, M.; Bhandari, B.; Yang, C.-h. Novel PH-Sensitive Films Containing Curcumin and Anthocyanins to Monitor Fish Freshness. *Food Hydrocolloids* **2020**, *100*, 105438.
(16) Khorasani, M. Y.; Langari, H.; Sany, S. B. T.; Rezayi, M.; Sahebkar, A. The Role of Curcumin and Its Derivatives in Sensory Applications. *Mater. Sci. Eng., C* **2019**, *103*, 109792.
(17) Zhou, X.; Yu, X.; Xie, F.; Fan, Y.; Xu, X.; Qi, J.; Xiong, G.; Gao, X.; Zhang, F. PH-Responsive Double-Layer Indicator Films Based on Konjac Glucomannan/Camellia Oil and Carrageenan/Anthocyanin/Curcumin for Monitoring Meat Freshness. *Food Hydrocolloids* **2021**, *118*, 106695.
(18) Roy, S.; Rhim, J.-W. Preparation of Bioactive Functional Poly(Lactic Acid)/Curcumin Composite Film for Food Packaging Application. *Int. J. Biol. Macromol.* **2020**, *162*, 1780−1789.
(19) Musso, Y. S.; Salgado, P. R.; Mauri, A. N. Smart Edible Films Based on Gelatin and Curcumin. *Food Hydrocolloids* **2017**, *66*, 8−15.
(20) Etxabide, A.; Maté, J. I.; Kilmartin, P. A. Effect of Curcumin, Betanin and Anthocyanin Containing Colourants Addition on Gelatin Films Properties for Intelligent Films Development. *Food Hydrocolloids* **2021**, *115*, 106593.
(21) Zhai, X.; Wang, X.; Zhang, J.; Yang, Z.; Sun, Y.; Li, Z.; Huang, X.; Holmes, M.; Gong, Y.; Povey, M.; Shi, J.; Zou, X. Extruded Low Density Polyethylene-Curcumin Film: A Hydrophobic Ammonia Sensor for Intelligent Food Packaging. *Food Packag. Shelf Life* **2020**, *26*, 100595.
(22) Pereira, P. F.; Andrade, C. T. Optimized PH-Responsive Film Based on a Eutectic Mixture-Plasticized Chitosan. *Carbohydr. Polym.* **2017**, *165*, 238−246.
(23) Quilez-Molina, A. I.; Pasquale, L.; Debellis, D.; Tedeschi, G.; Athanassiou, A.; Bayer, I. S. Responsive Bio-Composites from Magnesium Carbonate Filled Polycaprolactone and Curcumin-Functionalized Cellulose Fibers. *Adv. Sustain. Syst.* **2021**, *5*, 2100128.
(24) Sani, M. A.; Azizi-Lalabadi, M.; Tavassoli, M.; Mohammadi, K.; McClements, D. J. Recent Advances in the Development of Smart and Active Biodegradable Packaging Materials. *Nanomaterials* **2021**, *11*, 1331.
(25) Roy, S.; Priyadarshi, R.; Ezati, P.; Rhim, J.-W. Curcumin and Its Uses in Active and Smart Food Packaging Applications - A Comprehensive Review. *Food Chem.* **2022**, *375*, 131885.
(26) Zhang, J.; Huang, X.; Zou, X.; Shi, J.; Zhai, X.; Liu, L.; Li, Z.; Holmes, M.; Gong, Y.; Povey, M.; Xiao, J. A Visual Indicator Based on Curcumin with High Stability for Monitoring the Freshness of Freshwater Shrimp, Macrobrachium Rosenbergii. *J. Food Eng.* **2021**, *292*, 110290.
(27) Duan, M.; Yu, S.; Sun, J.; Jiang, H.; Zhao, J.; Tong, C.; Hu, Y.; Pang, J.; Wu, C. Development and Characterization of Electrospun Nanofibers Based on Pullulan/Chitin Nanofibers Containing Curcumin and Anthocyanins for Active-Intelligent Food Packaging. *Int. J. Biol. Macromol.* **2021**, *187*, 332−340.
(28) Yildiz, E.; Sumnu, G.; Kahyaoglu, L. N. Monitoring Freshness of Chicken Breast by Using Natural Halochromic Curcumin Loaded Chitosan/PEO Nanofibers as an Intelligent Package. *Int. J. Biol. Macromol.* **2021**, *170*, 437−446.
(29) Kim, M.; Lee, H.; Kim, M.; Park, Y. C. Coloration and Chromatic Sensing Behavior of Electrospun Cellulose Fibers with Curcumin. *Nanomaterials* **2021**, *11*, 222.
(30) Ma, X.; Chen, Y.; Huang, J.; Lv, P.; Hussain, T.; Wei, Q. In Situ Formed Active and Intelligent Bacterial Cellulose/Cotton Fiber Composite Containing Curcumin. *Cellulose* **2020**, *27*, 9371−9382.
(31) Bhargava, N.; Sharanagat, V. S.; Mor, R. S.; Kumar, K. Active and Intelligent Biodegradable Packaging Films Using Food and Food Waste-Derived Bioactive Compounds: A Review. *Trends Food Sci. Technol.* **2020**, *105*, 385−401.
(32) Ma, Q.; Lu, X.; Wang, W.; Hubbe, M. A.; Liu, Y.; Mu, J.; Wang, J.; Sun, J.; Rojas, O. J. Recent Developments in Colorimetric and

Optical Indicators Stimulated by Volatile Base Nitrogen to Monitor Seafood Freshness. *Food Packag. Shelf Life* **2021**, *28*, 100634.
(33) Pourjavaher, S.; Almasi, H.; Meshkini, S.; Pirsa, S.; Parandi, E. Development of a Colorimetric PH Indicator Based on Bacterial Cellulose Nanofibers and Red Cabbage (Brassica Oleraceae) Extract. *Carbohydr. Polym.* **2017**, *156*, 193−201.
(34) Zia, J.; Mancini, G.; Bustreo, M.; Zych, A.; Donno, R.; Athanassiou, A.; Fragouli, D. Porous PH Natural Indicators for Acidic and Basic Vapor Sensing. *Chem. Eng. J.* **2021**, *403*, 126373.
(35) Moradi, M.; Tajik, H.; Almasi, H.; Forough, M.; Ezati, P. A Novel PH-Sensing Indicator Based on Bacterial Cellulose Nanofibers and Black Carrot Anthocyanins for Monitoring Fish Freshness. *Carbohydr. Polym.* **2019**, *222*, 115030.
(36) Genovese, M. E.; Colusso, E.; Colombo, M.; Martucci, A.; Athanassiou, A.; Fragouli, D. Acidochromic Fibrous Polymer Composites for Rapid Gas Detection. *J. Mater. Chem. A* **2017**, *5*, 339−348.
(37) Prietto, L.; Pinto, V. Z.; El Halal, S. L. M.; de Morais, M. G.; Costa, J. A. V.; Lim, L.-T.; Dias, A. R. G.; Zavareze, E. d. R. Ultrafine Fibers of Zein and Anthocyanins as Natural PH Indicator. *J. Sci. Food Agric.* **2018**, *98*, 2735−2741.
(38) da Silva, C. K.; Mastrantonio, D. J. d. S.; Costa, J. A. V.; Morais, M. G. d. Innovative PH Sensors Developed from Ultrafine Fibers Containing Açaí (Euterpe Oleracea) Extract. *Food Chem.* **2019**, *294*, 397−404.
(39) Forghani, S.; Almasi, H.; Moradi, M. Electrospun Nanofibers as Food Freshness and Time-Temperature Indicators: A New Approach in Food Intelligent Packaging. *Innov. Food Sci. Emerg. Technol.* **2021**, *73*, 102804.
(40) Mohammadalinejhad, S.; Almasi, H.; Moradi, M. Immobilization of Echium Amoenum Anthocyanins into Bacterial Cellulose Film: A Novel Colorimetric PH Indicator for Freshness/Spoilage Monitoring of Shrimp. *Food Control* **2020**, *113*, 107169.
(41) Sun, W.; Liu, Y.; Jia, L.; Saldaña, M. D. A.; Dong, T.; Jin, Y.; Sun, W. A Smart Nanofibre Sensor Based on Anthocyanin/Poly-l-Lactic Acid for Mutton Freshness Monitoring. *Int. J. Food Sci. Technol.* **2021**, *56*, 342−351.
(42) Jadidi, A.; Salahinejad, E.; Sharifi, E.; Tayebi, L. Drug-Delivery Ca-Mg Silicate Scaffolds Encapsulated in PLGA. *Int. J. Pharm.* **2020**, *589*, 119855.
(43) Katsogiannis, K. A. G.; Vladisavljević, G. T.; Georgiadou, S. Porous Electrospun Polycaprolactone (PCL) Fibres by Phase Separation. *Eur. Polym. J.* **2015**, *69*, 284−295.
(44) Celebioglu, A.; Uyar, T. Electrospun Porous Cellulose Acetate Fibers from Volatile Solvent Mixture. *Mater. Lett.* **2011**, *65*, 2291−2294.
(45) Deng, Y.-F.; Zhang, D.; Zhang, N.; Huang, T.; Lei, Y.-Z.; Wang, Y. Electrospun Stereocomplex Polylactide Porous Fibers toward Highly Efficient Oil/Water Separation. *J. Hazard. Mater.* **2021**, *407*, 124787.
(46) Chen, Y.; Qiu, Y.; Chen, W.; Wei, Q. Electrospun Thymol-Loaded Porous Cellulose Acetate Fibers with Potential Biomedical Applications. *Mater. Sci. Eng., C* **2020**, *109*, 110536.
(47) Huang, C.; Thomas, N. L. Fabricating Porous Poly(Lactic Acid) Fibres via Electrospinning. *Eur. Polym. J.* **2018**, *99*, 464−476.
(48) Campagnolo, L.; Morselli, D.; Magrì, D.; Scarpellini, A.; Demirci, C.; Colombo, M.; Athanassiou, A.; Fragouli, D. Silk Fibroin/Orange Peel Foam: An Efficient Biocomposite for Water Remediation. *Adv. Sustainable Syst.* **2019**, *3*, 1800097.
(49) Mazzon, G.; Zahid, M.; Heredia-Guerrero, J. A.; Balliana, E.; Zendri, E.; Athanassiou, A.; Bayer, I. S. Hydrophobic Treatment of Woven Cotton Fabrics with Polyurethane Modified Aminosilicone Emulsions. *Appl. Surf. Sci.* **2019**, *490*, 331−342.
(50) Kossyvaki, D.; Suarato, G.; Summa, M.; Gennari, A.; Francini, N.; Gounaki, I.; Venieri, D.; Tirelli, N.; Bertorelli, R.; Athanassiou, A.; Papadopoulou, E. L. Keratin−Cinnamon Essential Oil Biocomposite Fibrous Patches for Skin Burn Care. *Mater. Adv.* **2020**, *1*, 1805−1816.
(51) Grum, F.; Witzel, R. F.; Stensby, P. Evaluation of Whiteness. *J. Opt. Soc. Am.* **1974**, *64*, 210−215.
(52) Mokrzycki, W.; Tatol, M. Color Difference Delta E - A Survey Colour Difference Δ E - A Survey Faculty of Mathematics and Informatics. *Mach. Graph. Vis.* **2011**, *20*, 383−411.
(53) Thommes, M.; Kaneko, K.; Neimark, A. V.; Olivier, J. P.; Rodriguez-reinoso, F.; Rouquerol, J.; Sing, K. S. W. Physisorption of Gases, with Special Reference to the Evaluation of Surface Area and Pore Size Distribution (IUPAC Technical Report). *Pure Appl. Chem.* **2015**, *87*, 1051−1069.
(54) Manolova, Y.; Deneva, V.; Antonov, L.; Drakalska, E.; Momekova, D.; Lambov, N. The Effect of the Water on the Curcumin Tautomerism: A Quantitative Approach. *Spectrochim. Acta, Part A* **2014**, *132*, 815−820.
(55) Hu, K.; Huang, X.; Gao, Y.; Huang, X.; Xiao, H.; McClements, D. J. Core-Shell Biopolymer Nanoparticle Delivery Systems: Synthesis and Characterization of Curcumin Fortified Zein-Pectin Nanoparticles. *Food Chem.* **2015**, *182*, 275−281.
(56) Mazzon, G.; Contardi, M.; Quilez-Molina, A.; Zahid, M.; Zendri, E.; Athanassiou, A.; Bayer, I. S. Antioxidant and Hydrophobic Cotton Fabric Resisting Accelerated Ageing. *Colloids Surf., A* **2021**, *613*, 126061.
(57) Stanić, Z. Curcumin, a Compound from Natural Sources, a True Scientific Challenge − A Review. *Plant Foods Hum. Nutr.* **2017**, *72*, 1−12.
(58) Bulushi, I. A.; Poole, S.; Deeth, H. C.; Dykes, G. A. Biogenic Amines in Fish: Roles in Intoxication, Spoilage, and Nitrosamine Formation-A Review. *Crit. Rev. Food Sci. Nutr.* **2009**, *49*, 369−377.
(59) Priyadarsini, K. I.; Maity, D. K.; Naik, G. H.; Kumar, M. S.; Unnikrishnan, M. K.; Satav, J. G.; Mohan, H. Role of Phenolic O-H and Methylene Hydrogen on the Free Radical Reactions and Antioxidant Activity of Curcumin. *Free Radic. Biol. Med.* **2003**, *35*, 475−484.
(60) Sharma, K.; Agrawal, S. S.; Gupta, M. Development and Validation of UV Spectrophotometric Method for the Estimation of Curcumin in Bulk Drug and Pharmaceutical Dosage Forms. *Int. J. Drug Dev. Res.* **2012**, *4*, 375−380.
(61) Van Nong, H.; Hung, L. X.; Thang, P. N.; Chinh, V. D.; Vu, L. V.; Dung, P. T.; Van Trung, T.; Nga, P. T. Fabrication and Vibration Characterization of Curcumin Extracted from Turmeric (Curcuma Longa) Rhizomes of the Northern Vietnam. *SpringerPlus* **2016**, *5*, 1147.
(62) Merrell, J. G.; Mclaughlin, S. W.; Tie, L.; Laurencin, C. T.; Chen, A. F.; Nair, L. S.; Phil, M.; Exp, C.; Author, P. P. Curcumin-loaded poly(ε-caprolactone) nanofibres: Diabetic wound dressing with anti-oxidant and anti-inflammatory properties. *Clin. Exp. Pharmacol. Physiol.* **2009**, *36*, 1149−1156.
(63) Juranić, I. Simple Method for the Estimation of pK_a of Amines. *Croat. Chem. Acta* **2014**, *87* (4), 343−347.
(64) Deng, H.; Zhu, J.; Tong, Y.; Kong, Y.; Tan, C.; Wang, M.; Wan, M.; Meng, X. Antibacterial Characteristics and Mechanisms of Action of Aronia Melanocarpa Anthocyanins against Escherichia Coli. *LWT* **2021**, *150*, 112018.
(65) Jongprakobkit, J.; Wisaichon, W.; Praditweangkum, W. A Simple and Green Approach for Colorimetric Ammonia Determination by Combining Pervaporation with Paper Impregnated Anthocyanins Extracted from Red Cabbage. *Curr. Appl. Sci. Technol.* **2020**, *20*, 394−407.
(66) Ulrich, S.; Moura, S. O.; Diaz, Y.; Clerc, M.; Guex, A. G.; de Alaniz, J. R.; Martins, A.; Neves, N. M.; Rottmar, M.; Rossi, R. M.; Fortunato, G.; Boesel, L. F. Electrospun Colourimetric Sensors for Detecting Volatile Amines. *Sens. Actuators, B* **2020**, *322*, 128570.
(67) Chignell, C. F.; Bilskj, P.; Reszka, K. J.; Motten, A. G.; Sik, R. H.; Dahl, T. A. Spectral and Photochemical Properties of Curcumin. *Photochem. Photobiol.* **1994**, *59*, 295−302.
(68) Rege, S. A.; Arya, M.; Momin, S. A. Structure Activity Relationship of Tautomers of Curcumin: A Review. *Ukr. Food J.* **2019**, *8*, 45−60.
(69) Singh, S.; Gaikwad, K. K.; Gaikwad, K. K.; Lee, Y. S. Anthocyanin − A Natural Dye for Smart Food Packaging Systems. *Korean J. Food Sci. Technol.* **2018**, *24*, 167−180.

https://doi.org/10.1021/acsapm.2c00418
ACS Appl. Polym. Mater. XXXX, XXX, XXX−XXX